The effect of oxygen content and cooling rate on phase transformations in directionally solidified intermetallic Ti-46Al-8Nb alloy

J. Lapin*, Z. Gabalcová

Institute of Materials and Machine Mechanics, Slovak Academy of Sciences, Račianska 75, 831 02 Bratislava, Slovak Republic

Abstract

The effect of oxygen content and cooling rate on phase transformations in directionally solidified (DS) intermetallic Ti-46Al-8Nb (at.%) alloy with columnar grain structure was studied. The phase transformations observed in the DS samples at various cooling rates are compared with those in the baseline as-received alloy with equiaxed grain structure. After solution annealing the baseline alloy with 500 wtppm oxygen as well as DS samples containing 1400, 1800 and 2500 wtppm were cooled to room temperature at various cooling rates ranging from 50 to about $1000 \, \text{K s}^{-1}$. The experimental results showed that the increase of oxygen content leads to a decrease in volume fraction of massively transformed γ_M(TiAl), an increase in volume fraction of retained α_R (Ti-based solid solution with hexagonal crystal structure) but has no significant effect on volume fraction of lamellar α_2(Ti$_3$Al) + γ(TiAl) microstructure at constant cooling rate. Increase of cooling rate leads to a decrease in volume fraction of massive γ_M and an increase in volume fraction of retained α_R at constant oxygen content. Cooling rates corresponding to oil and water quenching can suppress formation of lamellar $\alpha_2 + \gamma$ microstructure. Nucleation and growth of massive γ_M is significantly enhanced within parent α grains when the nucleation at the grain boundaries is suppressed by stabilization of the α-phase by oxygen at low cooling rates. Vickers microhardnesses HV$_m$ of massive γ_M as well as of retained α_R increase with increasing oxygen content and cooling rate.

K e y   w o r d s: titanium aluminides, TiAl, heat treatment, phase transformations, microstructure, mechanical properties

1. Introduction

Since the last two decades, TiAl-based alloys have attracted attention as potential candidates for high--temperature structural applications in the aerospace and automotive industries [1–8]. Due to low density, high specific strength, high Young's modulus retention and oxidation resistance at high temperatures, these materials represent good alternatives to currently used nickel-based alloys [9–11] and superior high temperature mechanical properties when compared to classical Ti-based alloys [12, 13]. Besides increase of low room--temperature ductility and fracture toughness, suc-

cessful industrial application of TiAl-based alloys is conditioned also by development of economical processing routes. Among various processing techniques, precise casting represents very promising technology for production of complex shaped components with a competitive price when compared to those of nickel--based superalloys [14]. On the other hand, coarse-grained structure and higher oxygen content in cast components lead to low room-temperature ductility, fracture toughness and large scatter of mechanical properties. There are two main approaches how to refine coarse-grained structure of cast TiAl-based alloys: (i) affecting solidification path by alloying with boron

[15, 16] and (ii) through solid state transformations by appropriate post-solidification heat treatments. According to the importance of diffusion, the solid state phase transformations in TiAl-based alloys can be divided into two groups: (i) diffusionless massive transformation which involves atoms transfer across the interface between the parent α-phase (Ti-based solid solution with hexagonal crystal structure) and the massive γ_M-TiAl and (ii) diffusion-related transformations leading to formation of $\alpha + \gamma$ two-phase microstructures such as lamellar, Widmanstätten lamellar and feathery structures where two phases have different chemical compositions [17–20]. The massive transformation strongly depends on content of Al and O. In alloys with Al contents below about 45 at.% the stability of α-phase is increased and rapid quenching leads to the retention of α-phase to room temperature (in the form of ordered α_2-Ti$_3$Al) rather than to formation of massive γ_M. Correspondingly, high oxygen contents can suppress the massive transformation even in alloys containing 48 at.% of Al [21]. As shown recently by Huang et al. [22] for Ti-46Al-8Nb (at.%) alloy with equiaxed grain structure (grain size of about 1000 μm), increase of oxygen content from 500 to 1500 wtppm can suppress the massive transformation at high cooling rates and affects significantly phase transformations at lower cooling rates. However, it is not clear how various oxygen contents affect phase transformations in an alloy with columnar grain structure which is usually formed in large complex shaped components such as turbine blades during casting [23, 24]. Such information is of a great interest to define processing windows including melting, casting and post-solidification heat treatments of TiAl-based alloys with Al content higher than 45 at.% which coarse-grained structure is to be refined through massive transformation.

The aim of this paper is to study the effect of oxygen content and cooling rate on phase transformations in directionally solidified (DS) intermetallic Ti-46Al-8Nb (at.%) alloy with columnar grain structure. The phase transformations observed in DS samples are compared with those in the baseline as-received alloy with equiaxed grain structure at various cooling rates. The studied alloy has been selected as a potential material for the investment casting of low pressure turbine blades of aircraft engines and stationary gas turbines for power engineering [25]. In this alloy, the addition of 8 at.% of Nb with diffusion coefficient of about one order lower than that of Ti in both TiAl and Ti$_3$Al, stabilizes β phase (Ti-based solid solution with cubic crystal structure) and improves high oxidation resistance [25–27]. Addition of 46 at.% of Al guarantees grain refinement of the as-cast microstructures through massive transformation of the α-phase to massive γ_M during cooling from single α-phase field [27].

2. Experimental procedure

The intermetallic alloy with the chemical composition Ti-46Al-8Nb (at.%) and initial oxygen content of 500 wtppm was supplied in the form of vacuum arc re-melted cylindrical ingot with a diameter of 220 mm and a length of 60 mm. The ingot was cut to smaller blocks using electro spark machining, lathe machined to a diameter of 8 mm and length of 110 mm and directionally solidified in dense cylindrical Y$_2$O$_3$ moulds (purity of 99.5 %) with a diameter of 8/12 (inside/outside diameter) and length of 130 mm. Before directional solidification the vacuum chamber of the apparatus was evacuated to a pressure of 3 Pa, flushed with argon (purity 99.9995 %) six times and then backfilled with argon at a pressure of 10 kPa, which was held constant during melting and solidification. Directional solidification was performed at three constant growth rates V of 5.56×10^{-6}, 5.56×10^{-5} and 1.18×10^{-4} m s^{-1} in a modified Bridgman-type apparatus described elsewhere [28].

Samples for heat treatments with a diameter of 8 mm and a length of 10 mm were cut from the baseline as-received alloy and DS samples. After cutting, the samples were solution annealed at a temperature of 1633 K (α-phase field) for 1 h in a dynamic argon atmosphere and subsequently cooled to room temperature by free air cooling (AC), compressed air cooling (CC), oil quenching (OQ) and water quenching (WQ). Cooling rates for heat treated (HT) samples were measured using computer data acquisition system with Pt-PtRh10 thermocouple placed in a sample hole with a diameter of 2.5 mm and length of 2 mm drilled specially for cooling rate measurements. The cooling rates corresponding to AC, CC, OQ and WQ were measured to be 50, 250, ~ 600 and ~ 1000 K s^{-1}, respectively.

Oxygen content was measured with a LECO TC-436 N/O apparatus. Before oxygen measurements, the apparatus was calibrated using standards with certified oxygen content. The analysed specimens with a diameter of 8 mm and length of 20 mm were cut from DS samples. The surface layer was removed by grinding and the specimens were carefully drilled to achieve fine chips for oxygen measurements. The melting (burning) of chips was performed in a graphite crucible under helium. Oxygen was detected in the form of carbon dioxide using infrared detection.

Vickers microhardness measurements of DS and HT samples were performed at a load of 0.42 N. The loading time was 10 s.

Microstructural analysis was performed by light optical microscopy (OM). OM samples were prepared using standard metallographic techniques and etched in a reagent of 50 ml H$_2$O, 3 ml HNO$_3$ and 1.5 ml HF.
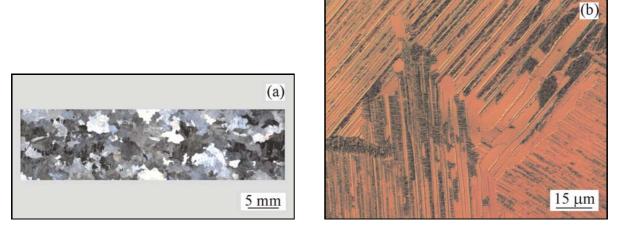
Fig. 1. (a) Equiaxed grain structure of baseline as-received alloy with oxygen content of 500 wtppm. (b) OM micrograph showing lamellar $\alpha_2 + \gamma$ microstructure within equiaxed grains.
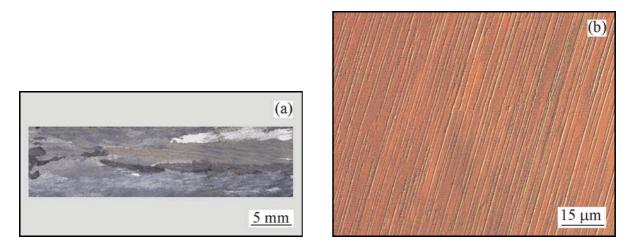

Fig. 2. (a) Columnar grain structure on longitudinal section of DS sample prepared at $V = 5.56 \times 10^{-5}\,\mathrm{m\,s^{-1}}$, $G_L = 5 \times 10^3\,\mathrm{K\,m^{-1}}$ and oxygen content of 1800 wtppm. (b) OM micrograph showing lamellar $\alpha_2 + \gamma$ microstructure within columnar grains.

Quantitative metallographic analysis was performed on digitalized micrographs using a computerized image analyser.

3. Results

3.1. Microstructure before heat treatments

Figure 1 shows the typical examples of macrostructure and microstructure of samples prepared from the baseline as-received ingot with an initial oxygen content of 500 wtppm. The sample consists of equiaxed grains with an average grain size of 1600 µm, as shown in Fig. 1a. The microstructure within the equiaxed grains is fully lamellar and consists of γ(TiAl) and α_2(Ti$_3$Al) phases, as seen in Fig. 1b.

The aim of directional solidification experiments

was to prepare samples with columnar grain structure and various oxygen contents. As shown recently by Lapin et al. [29], during directional solidification in Y_2O_3 moulds oxygen content in DS samples increases with increasing reaction time and temperature of the melt. The reaction time depends on withdrawal rate and sample holding time before its withdrawal from the hot zone of the furnace. For the purpose of this work, various oxygen contents in DS samples were achieved by variation of reaction time from 2000 to 12900 s at two maximum melt temperature values of 1933 and 1973 K. Such parameters of directional solidification resulted in a measured oxygen content of 1400, 1800 and 2500 wtppm in the DS samples prepared at V of 1.18×10^{-4}, 5.56×10^{-5} and $5.56 \times 10^{-6}\,\mathrm{m\,s^{-1}}$, respectively. Figure 2 shows the typical examples of macrostructure and microstructure of samples after directional solidification. The samples contain several columnar grains with an av-
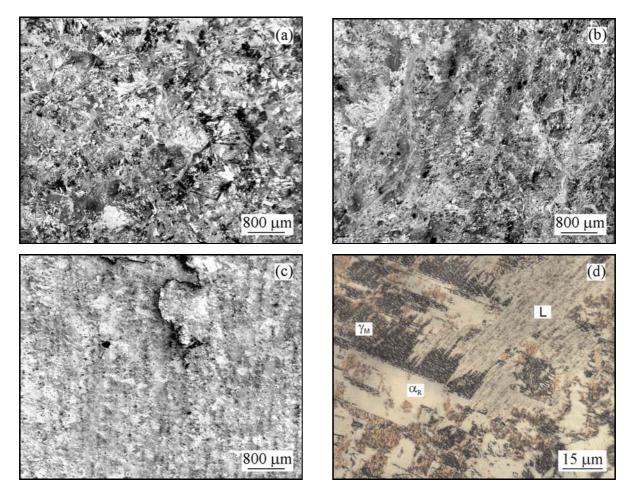
Fig. 3. OM micrographs showing influence of oxygen content on the microstructure of samples after free air cooling (AC): (a) 500 wtppm oxygen – equiaxed structure; (b) 1400 wtppm oxygen – longitudinal section; (c) 2500 wtppm oxygen – longitudinal section; (d) 2500 wtppm oxygen – longitudinal section, L – lamellar microstructure, α_R – retained α, γ_M – massively transformed γ.

erage diameter of 1700 µm elongated in a direction nearly parallel to its longitudinal axis, as shown in Fig. 2a. The microstructure within columnar grains consists of γ and α_2 lamellae, as seen in Fig. 2b.
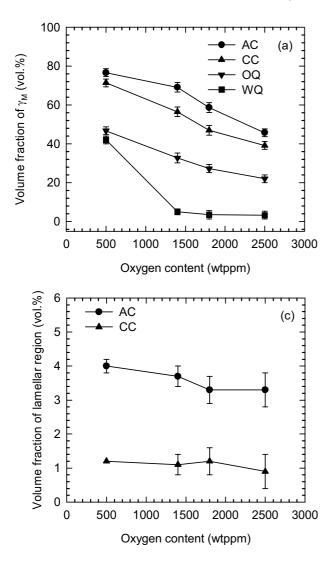
3.2. Microstructure after heat treatments

3.2.1. Air cooling

Figure 3 shows influence of free air cooling (AC) on the microstructure of the HT samples with various oxygen contents. The microstructure of the samples containing 500 wtppm oxygen (Fig. 3a) is similar to that of the samples containing 1400 wtppm (Fig. 3b) or 2500 wtppm (Fig. 3c). During the heat treatment the columnar grain structure fully transformed to equiaxed grains due to transformation of α-phase to massive γ_M. Increase of oxygen content to 2500 wtppm resulted in cracking of the samples during cooling, as shown in Fig. 3c. Generally, each of the samples subjected to AC contained three microstructurally dif-

ferent regions, which could be clearly distinguished and quantified by the means of optical microscopy: (i) massive γ_M, (ii) retained α_R and (iii) lamellar $\alpha_2 + \gamma$ microstructure, as shown in Fig. 3d. Figure 4 shows evolution of volume fraction of massive γ_M, retained α_R and lamellar $\gamma + \alpha_2$ microstructure with the oxygen content. During AC the increase of oxygen content from 500 to 2500 wtppm leads to a decrease of volume fraction of massive γ_M by 31 vol.% (Fig. 4a), an increase of volume fraction of retained α_R by 31 vol.% (Fig. 4b) but has no significant effect on volume fraction of lamellar $\alpha_2 + \gamma$ microstructure (Fig. 4c).

3.2.2. Compressed air cooling

Figure 5 shows influence of compressed air cooling (CC) on the microstructure of the samples with various oxygen content. Figure 5a shows the typical microstructure of the samples with equiaxed grain structure and oxygen content of 500 wtppm after compressed air cooling. The microstructure consists of massive γ_M, retained α_R and small amount of lamellar $\alpha_2 + \gamma$. Similar
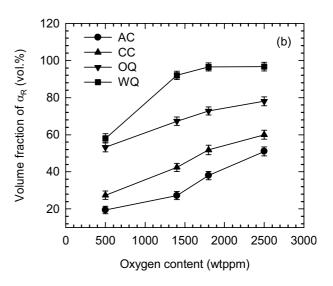
Fig. 4. Dependence of volume fraction of coexisting regions on oxygen content: (a) massive γ_M; (b) retained α_R and (c) lamellar $\alpha_2 + \gamma$ microstructure. The cooling rates are indicated in the figure.

microstructures are observed for the DS samples with columnar grain structure and oxygen content of 1400 or 1800 wtppm, as seen in Figs. 5b and 5c. Increase of oxygen content in the DS samples to 2500 wtppm stabilizes large volume fraction of retained α_R in the microstructure, as seen in Fig. 5d. During CC the increase of oxygen content from 500 to 2500 wtppm leads to a decrease of volume fraction of massive γ_M by 32 vol.% (Fig. 4a), increase of volume fraction of retained α_R by 33 vol.% (Fig. 4b) but has no significant effect on volume fraction of lamellar $\alpha_2 + \gamma$ microstructure (Fig. 4c).

3.2.3. Oil quenching

Figure 6 shows influence of oil quenching (OQ) on the microstructure of the samples with various oxygen contents. The microstructure of the samples containing 500 wtppm oxygen (Fig. 6a) is significantly different from that of the samples containing 1400 wtppm (Fig. 6b), 1800 wtppm (Fig. 6c) or 2500 wtppm (Fig. 6d). During OQ the increase of

oxygen content in the DS samples stabilizes retained α_R in the microstructure. While the samples with 1400 wtppm oxygen (Fig. 6b) show intensive nucleation of massive γ_M also within the columnar grains, the samples with 1800 and 2500 wtppm oxygen transformed massively preferentially along the columnar grain boundaries and very limited amount of massive γ_M was nucleated within the α grains. Such limited massive transformation preserved the columnar grain structure with high anisotropy. Each of the samples subjected to OQ contained only two microstructurally different regions, which could be clearly distinguished and quantified by the means of optical microscopy: (i) massive γ_M and (ii) retained α_R. The increase of oxygen content from 500 to 2500 wtppm leads to a decrease of volume fraction of massive γ_M by 25 vol.% (Fig. 4a) and an increase of volume fraction of retained α_R by 25 vol.% (Fig. 4b).

3.2.4. Water quenching

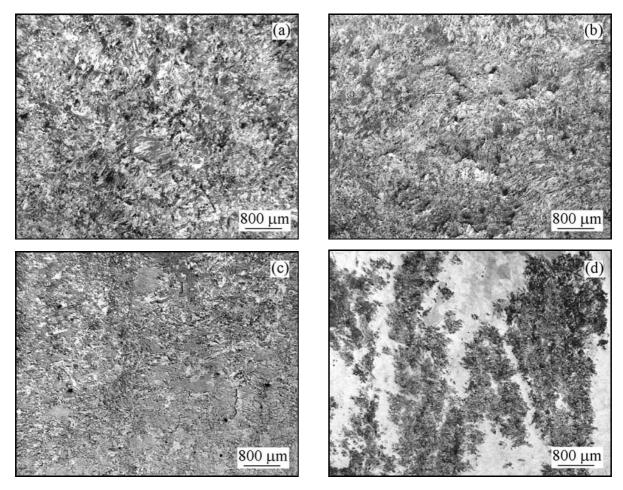Figure 7 shows influence of water quenching (WQ)

Fig. 5. OM micrographs showing influence of oxygen content on the microstructure of samples after compressed air cooling (CC): (a) 500 wtppm oxygen; (b) 1400 wtppm oxygen – longitudinal section; (c) 1800 wtppm oxygen – longitudinal section; (d) 2500 wtppm oxygen – longitudinal section.

on microstructure of the heat-treated samples. The microstructures of the samples containing 500 wtppm oxygen (Fig. 7a) as well as the samples containing 1400 wtppm (Fig. 7b), 1800 wtppm (Fig. 7c) or 2500 wtppm (Fig. 7d) contain numerous cracks. During WQ the increase of oxygen content in the DS samples stabilizes retained α_R in the microstructure. The DS samples show nucleation of massive γ_M along the columnar grain boundaries and only very limited amount of γ_M is formed within the grains. As in the case of OQ, such limited massive transformation preserved the columnar grain structure with high anisotropy. Each of the samples subjected to WQ contained only two microstructurally different regions: (i) massive γ_M and (ii) retained α_R. The increase of oxygen content from 500 to 2500 wtppm leads to a decrease of volume fraction of massive γ_M by 39 vol.% (Fig. 4a) and an increase of volume fraction of retained α_R by 39 vol.% (Fig. 4b).

3.3. Vickers microhardness

Figure 8 shows variation of Vickers microhardness with oxygen content. The microhardnesses HV_m of massive γ_M (Fig. 8a) as well as of retained α_R (Fig. 8b) increase with increasing oxygen content and cooling rate. The microhardness of lamellar $\alpha_2 + \gamma$ microstructure could not be reliably measured since the size of lamellar regions was smaller than the indentation size in the HT samples.

The Vickers microhardnesses HV_m of the massive γ_M as well as of retained α_R in the HT samples can be also compared with microhardness values measured in the DS samples before their heat treatment. Figures 8a and 8b show average maximum ($HV_{m1400} = 4.9$ GPa) and minimum ($HV_{m2500} = 4.1$ GPa) microhardness values which were measured in the DS samples with oxygen content of 1400 wtppm and 2500 wtppm, respectively. The microhardness value of 4.3 GPa measured in the DS samples with oxygen content of 1800 wtppm falls very well between these upper and lower microhardness limits. Assuming these measured microhardness values, it seems that the increase of oxygen content leads apparently to a softening of the DS samples after directional solidification. However, after the heat treatment of the DS samples, the
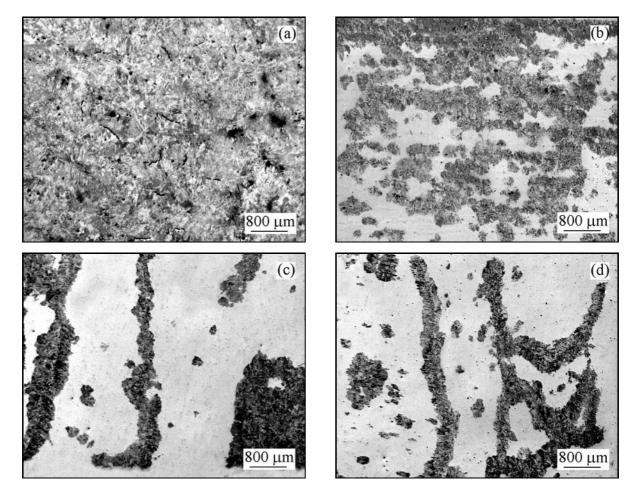
Fig. 6. OM micrographs showing influence of oxygen content on the microstructure of samples after oil quenching (OQ): (a) 500 wtppm oxygen; (b) 1400 wtppm oxygen – longitudinal section; (c) 1800 wtppm oxygen – longitudinal section; (d) 2500 wtppm oxygen – longitudinal section.

microhardness increases with increasing oxygen content. This discrepancy between the evolution of microhardness in the DS and HT samples with oxygen content can be explained by fully lamellar $\alpha_2 + \gamma$ microstructure of the DS samples. As shown by Lapin et al. [28], Vickers microhardness of DS samples depends on interlamellar α_2-α_2 spacing and increases with decreasing interlamellar spacing. The interlamellar α_2-α_2 spacing in the DS samples containing 1400, 1800 and 2500 wtppm oxygen was measured to be 0.55, 1.19 and 2.21 µm and decreased with increasing growth rate. Hence, the apparent softening of the DS samples with increasing oxygen content is caused by coarser lamellar $\alpha_2 + \gamma$ microstructure contribution of which to the overall measured microhardness is larger than strengthening resulting from increasing content of interstitial atoms of oxygen.

4. Discussion

4.1. Effect of cooling rate and oxygen on phase transformations

The microstructure observations of the baseline as well as DS samples are in a good agreement with the results reported for ternary Ti-46Al-8Nb or binary Ti-48Al (at.%) alloys with equiaxed grain structure and various oxygen contents [18, 22]. Figure 9 shows schematic continuous cooling transformation (CCT) diagram suggested by Huang et al. [22] for Ti-46Al--8Nb (at.%) alloy with equiaxed grain structure. Figure 9a indicates the position of cooling curves corresponding to AC, CC, OQ and WQ applied in this work which was estimated from the microstructure analysis of the HT baseline samples with equiaxed grain structure containing 500 wtppm oxygen. As seen in this figure, higher cooling rates corresponding to OQ and WQ fall into region of diffusionless phase transformation leading to formation of two-phase $\alpha_R + \gamma_M$ type of microstructure. As results from the microstructures shown in Figs. 6a and 7a as well as from the quantitative metallographic analysis summarized in Figs. 4a and 4b, such high cooling rates stabilize relatively high volume fraction of retained α_R which leads to stabilization of some relatively large α (in the form of α_2) grains
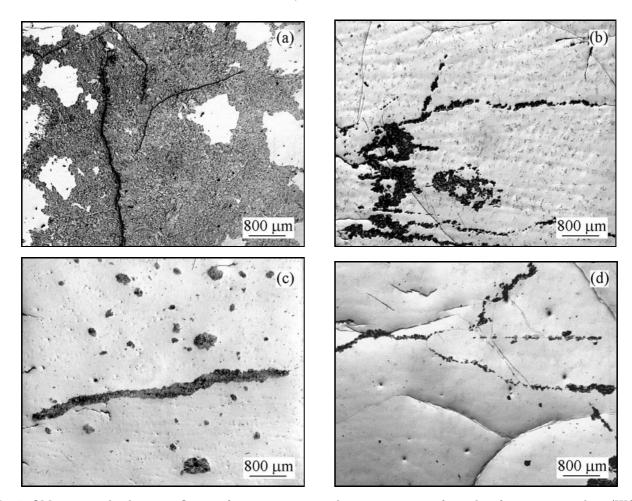
Fig. 7. OM micrographs showing influence of oxygen content on the microstructure of samples after water quenching (WQ):
(a) 500 wtppm oxygen; (b) 1400 wtppm oxygen – longitudinal section; (c) 1800 wtppm oxygen – longitudinal section; (d)
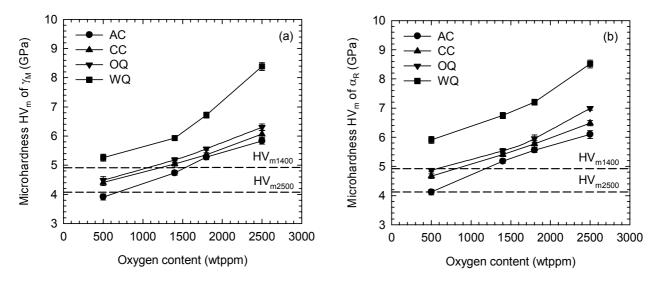2500 wtppm oxygen – longitudinal section.

Fig. 8. Dependence of Vickers microhardness on oxygen content: (a) massive γ_M and (b) retained α_R. The cooling rates
are indicated in the figure.

after the heat treatment. Lower cooling rates corres-
ponding to AC and CC regimes fall into diffusion-

less and diffusion-related region of phase transforma-
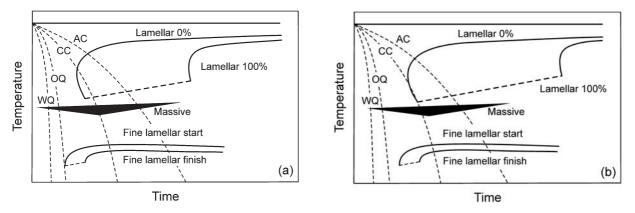tions leading to formation of massive γ_M and lamellar

Fig. 9. Schematic continuous cooling transformation (CCT) diagram for Ti-46Al-8Nb (at.%) alloy according to Huang et al. [22]: (a) 500 wtppm oxygen – equiaxed grain structure; (b) 2500 wtppm oxygen – columnar grain structure. The applied cooling rates corresponding to AC, CC, OQ and WC are indicated in the figure.
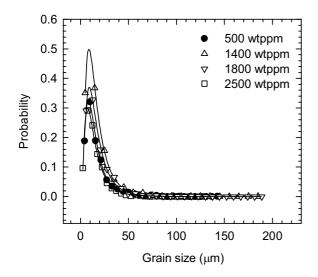

Fig. 10. Log-normal distribution curves of measured grain size in baseline and DS samples after AC. The oxygen contents are indicated in the figure.

$\alpha_2 + \gamma$ microstructure. At all applied cooling rates, the CCT diagram indicates formation of fine lamellar microstructure, which was observed at columnar grain boundaries.

Microstructure analysis of the DS samples with columnar grain structure revealed that the position of diffusionless phase transformation region in the CCT diagram strongly depends on the oxygen content. Since oxygen is stabilizer of the α-phase, increase of oxygen content decreases cooling rates required for diffusionless massive transformation and retards diffusion related formation of coarse lamellar $\alpha_2 + \gamma$ microstructure. Figure 9b shows schematically the effect of 2500 wtppm oxygen on the CCT diagram and indicates the cooling rates corresponding to AC, CC, OQ and WQ applied in this work. In this diagram, the diffusionless region is shifted to significantly lower cooling rates. Even the cooling rate corresponding to

CC falls into this region and preserves high volume fraction of retained α_R in the microstructure, as seen in Fig. 5d. As results from the microstructure observations, the only possible way of the grain refinement in the samples with the highest oxygen content is to decrease cooling rate to achieve diffusionless and diffusion-related region of phase transformations. Stabilization of large retained α_R regions at high cooling rates results in preservation of large grains after the heat treatment.

4.2. Effect of massive transformation on grain size

As shown by several authors [30–32], massive transformation of the α-phase to massive γ_M results in fine grain structure due to formation of many small subgrains by successive twinning of growing massively transformed γ_M. Huang et al. [26] have shown that the subgrains formed by twinning have no simple crystallographic orientation relation with the parent α-phase and the loss of any orientation relationship is caused also by formation of high angle boundaries between the growing regions of massive γ_M. On the other hand, Dey et al. [31] have confirmed Blackburn crystallographic orientation relationship, i.e. $(0002)_\alpha \parallel (111)_\gamma$ and $[11\bar{2}0]_\alpha \parallel [1\bar{1}0]_\gamma$, between massive γ_M grains and one of the two parent α grains during nucleation and growth of the massive γ_M. In spite of a large discrepancy among experimental studies concerning crystallographic orientation relationships between the parent α-phase and massive γ_M grains, there are no doubts that the α–α grain boundaries are preferential nucleation sites for massive γ_M in many TiAl-based alloys. Hence, assuming constant oxygen content, higher volume fraction of massive γ_M is expected in the samples with equiaxed grain structure than in those with columnar grain structure before the heat treatments. Huang et al. [22] have observed that the local oxygen level increases at grain boundaries during cool-

ing at slow rates and such higher oxygen content stabilizes the α-phase so that massive transformation can be suppressed locally. Figure 4a supports these qualitative observations and clearly shows quantitatively that the increase of oxygen content in the DS samples with columnar grain structure decreases volume fraction of massive γ_M after AC of HT samples. It should be noted that the cooling rate of $50\,\mathrm{K\,s^{-1}}$ measured for AC is relatively high and results from small size of the samples and their enhanced cooling caused by an intensive extraction of heat by a metallic perforated support used during the heat treatments. Figure 10 shows the effect of oxygen content on log-normal distribution curves resulting from statistical evaluation of grain size in the samples subjected to AC. Comparison of mean values of the grain size ranging between 7.4 and 9.1 μm or maximum measured values of grain size ranging between 150 and 190 μm, one can find no significant effect of the increase of oxygen content or columnar grain structure on the grain refinement during AC. This analysis clearly shows that a relatively low volume fraction of massive γ_M (46 vol.%) is also sufficient to refine columnar grain structure of the samples containing 2500 wtppm oxygen similarly to that of the samples with equiaxed grain structure containing 76 vol.% of massive γ_M and only 500 wtppm. The metallographic observations strongly suggest that such high efficiency of lower volume fraction of massive γ_M in the grain refinement results from enhanced nucleation and growth of massive γ_M regions within the α grains. Nucleation of massive γ_M within α grains occurs at defects such as dislocations and stacking faults and its probability is significantly increased when the nucleation at the grain boundaries is suppressed by stabilization of the α-phase due to higher oxygen content [22]. The enhanced nucleation and growth of massive γ_M within the α grains can be clearly seen in the DS samples with 1400 wtppm oxygen shown in Fig. 6b. It should be noted that CC, OQ and WQ regimes resulted in large volume fraction of retained α_R, which was connected with preservation of large grains ranging from 800 to 2000 μm in the microstructure, which could not be included to the statistical analysis.

5. Conclusions

The investigation of the effect of oxygen content and cooling rate on phase transformations in DS Ti-46Al-8Nb (at.%) alloy with columnar grain structure suggests the following conclusions:

1. Increase of oxygen content from 500 to 2500 wtppm leads to a decrease in volume fraction of massive γ_M, an increase in volume fraction of retained α_R but has no significant effect on volume fraction of lamellar $\alpha_2 + \gamma$ microstructure at constant cooling rate.

2. Increase of cooling rate from 50 to about $1000\,\mathrm{K\,s^{-1}}$ leads to a decrease in volume fraction of massive γ_M and an increase in volume fraction of retained α_R at constant oxygen content. Cooling rates corresponding to OQ and WQ can suppress formation of lamellar $\alpha_2 + \gamma$ microstructure.

3. Nucleation and growth of massive γ_M is significantly enhanced within parent α grains when the nucleation at the grain boundaries is suppressed by stabilization of the α-phase by oxygen at low cooling rates.

4. Vickers microhardnesses HV_m of massive γ_M as well as of retained α_R increase with increasing oxygen content and cooling rate.

References

[1] LORIA, E. A.: Intermetallics, *8*, 2000, p. 1339.
[2] TETSUI, T.: Mater. Sci. Eng. A, *329–331*, 2002, p. 582.
[3] SANIN, V.—YUKHVID, V.—SYTSCHEV, A.—ANDREEV, D.: Kovove Mater., *44*, 2006, p. 49.
[4] LAPIN, J.—GABALCOVÁ, Z.—BAJANA, O.—DALOZ, D.: Kovove Mater., *44*, 2006, p. 297.
[5] LAPIN, J.: Kovove Mater., *44*, 2006, p. 57.
[6] GABALCOVÁ, Z.—LAPIN, J.: Kovove Mater., *45*, 2007, p. 177.
[7] LAPIN, J.—PELACHOVÁ, T.—DOMÁNKOVÁ, M.—DALOZ, D.—NAZMY, M.: Kovove Mater., *45*, 2007, p. 121.
[8] AGOTE, I.—COLETO, J.—GUTIERREZ, M.—SARGSYAN, A.—GARCIA DE CORTAZAR, M.—LAGOS, M. A.—KVANIN, V. L.—BALIKHINA, N. T.—VADCHENKO, S. G.—BOROVINSKAYA, I. P.—SYTSCHEV, A. E.—PAMBAGUIAN, L.: Kovove Mater., *46*, 2008, p. 87.
[9] KUNZ, L.—LUKÁŠ, P.—MINTÁCH, R.—HRBÁČEK, K.: Kovove Mater. *44*, 2006, p. 275.
[10] HAKL, J.—VLASÁK, T.—LAPIN, J.: Kovove Mater., *45*, 2007, p. 177.
[11] LAPIN, J.—MAREČEK, J.—KURSA, M.: Kovove Mater., *44*, 2006, p. 1.
[12] MOSKALEWICZ, T.—ZIMOWSKI, S.—KITANO, Y.—WIERZCHON, T.—CZYRSKA-FILEMONOWICZ, A.: Kovove Mater., *44*, 2006, p. 133.
[13] KUDRMAN, J.—FOUSEK, J.—BŘEZINA, V.—MÍKOVÁ, R.—VESELÝ, J.: Kovove Mater., *45*, 2007, p. 199.
[14] HARDING, R. A.: Kovove Mater., *42*, 2004, p. 225.
[15] CHENG, T. T.: Intermetallics, *8*, 2000, p. 29.

[16] CHENG, T. T.—WILLIS, M. R.—JONES, I. P.: Intermetallics, *7*, 1999, p. 89.

[17] ZHANG, X. D.—GODFREY, S.—WEAVER, M.—STRANGWOOD, M.—THREADGILL, P.—KAUFMAN, M. J.—LORETTO, M. H.: Acta Mater., *44*, 1996, p. 3723.

[18] PRASAD, U.—CHATURVEDI, M. C.: Metall. Mater. Trans. A, *34A*, 2003, p. 2053.

[19] DENQUIN, A.—NAKA, S.: Acta Mater., *44*, 1996, p. 353.

[20] VEERARAGHAVAN, D.—WANG, P.—VASUDEVAN, V. K.: Acta Mater., *47*, 1999, p. 3313.

[21] LEFEBVRE, W.—LOISEAU, A.—MENAND, A.: Metall. Trans. A, *34A*, 2003, p. 2067.

[22] HUANG, A.—LORETTO, M. H.—HU, D.—LIU, K.—WU, X.: Intermetallics, *14*, 2006, p. 838.

[23] LAPIN, J.—KLIMOVÁ, A.: Kovove Mater., *41*, 2003, p. 1.

[24] LAPIN, J.—NAZMY, M.:. Mater. Sci. Eng. A, *380*, 2004, p. 298.

[25] JARVIS, D. J.—VOSS, D.: Mat. Sci. Eng. A, *413–414*, 2005, p. 583.

[26] HUANG, A.—HU, D.—WU, X.—LORETTO, M. H.: Intermetallics, *15*, 2007, p. 1147.

[27] HU, D.—HUANG, A. J.—WU, X.: Intermetallics, *15*, 2007, p. 327.

[28] LAPIN, J.—ONDRÚŠ, Ľ.—NAZMY, M.: Intermetallics, *10*, 2002, p. 1019.

[29] LAPIN, J.—PELACHOVÁ, T.—GABALCOVÁ, Z.: submitted to J. Mater. Sci.

[30] VEERARAGHAVAN, D.—WANG, P.—VASUDEVAN, V. K.: Acta Mater., *51*, 2003, p. 1721.

[31] DEY, S. R.—BOUZY, E.—HAZOTTE, A.: Intermetallics, *14*, 2006, p. 444.

[32] DENQUIN, A.—NAKA, S.: Acta Mater., *44*, 1996, p. 343.